Arabian Journal of Geosciences (2021) 14: 1660
https://doi.org/10.1007/s12517-021-08043-w

ORIGINAL PAPER

Petrology and geochronology of metamorphic rocks from the Bossangoa-Bossembélé area, Northern Central African Republic—evidence for Palaeoproterozoic high-grade metamorphism in the North Equatorial Fold Belt

Evine Laure Tanko Njiosseu[1] · Prince Emilien Danguene[2] · Timoleon Ngnotue[1] · Sylvestre Ganno[3] · Gus Djibril Kouankap Nono[4] · Christiane Diorlette Ngo Nlend[5] · Boniface Kankeu[6] · Jean Biandja[2] · Jean Paul Nzenti[3]

Received: 18 February 2021 / Accepted: 15 July 2021 / Published online: 4 August 2021

Abstract

Metamorphic rocks of the Bossangoa-Bossembélé area in the northern Central African Republic (CAR) consist of both meta-sedimentary and meta-igneous units. A petrographic investigation reveals that the meta-sedimentary unit is composed of pelitic granulites while meta-igneous unit comprises mafic granulites. The mineral assemblages are indicative of granulite facies conditions (i.e., Cpx–Opx–Grt–Qtz–Pl in meta-igneous unit, and Grt-Pl-Sill-Qtz in meta-sedimentary unit). The REE patterns of the pelitic granulites are fractionated with strong positive Eu (Eu/Eu*= 13.75–18.59) anomalies. The meta-igneous rocks display the chemical composition of diorite with CaO/TiO_2 (3.71–4.80), Al_2O_3/TiO_2 (>12), and Y/Nb (>1) elemental ratios similar to those of tholeiites. Their REE patterns display negative (Eu/Eu* = 0.44–0.86) Eu anomalies. SHRIMP U-Pb zircon data indicated that the peak HP-HT metamorphic conditions were reached during the Eburnean/Transamazonian orogeny at ca. 1952 Ma. The studied rocks were later affected by the Pan-African orogeny at 640.8 ± 6.0 Ma. The new findings indicate that the Pan-African sedimentary series were deposited on an old Paleoproterozoic continental crust. The metamorphic rocks of Bossangoa-Bossembélé area share strong similarities with high-grade gneisses of Cameroon, eastern Nigeria, and NE Brazil. This suggests that the Bossangoa-Bossembélé and Nyong and Ogooué series are the extension in central Africa of the Transamazonian belt.

Keywords HP-HT metamorphism · Gneiss · SHRIMP U-Pb age · Paleoproterozoic · Pan-African · CAR

Responsible Editor: Domenico M. Doronzo

✉ Evine Laure Tanko Njiosseu
rnelly2013@gmail.com

[1] Department of Earth Sciences, University of Dschang, P.O. Box 67, Dschang, Cameroon

[2] Department of Earth Sciences, University of Bangui, P.O. Box 908, Bangui, Central African Republic

[3] Department of Earth Sciences, University of Yaoundé I, P.O. Box 812, Yaoundé, Cameroon

[4] Department of Geology, HTTC, University of Bamenda, P.O. Box 39, Bambili, Bamenda, Cameroon

[5] Institute of Mineralogy and Geochemistry, University of Lausanne, Anthropole, CH-1015 Lausanne, Switzerland

[6] Institute for Geological and Mining Researches (IGMR), P.O. Box 4110, Yaounde, Cameroon

Introduction

The Bossangoa-Bossembélé area is located on the central part of the CAR in the North Equatorial Fold Belt (NEFB) (Danguene et al. 2014). Although the western extension towards the Yade-Adamawa area is still poorly known, the study of Yade-Adamawa region is of particular interest in deciphering the true nature of the fold belt as it corresponds to the transition between the northern margin of the Congo Craton (CC) and the Neoproterozoic domain. The zone towards the Yade-Adamawa region is considered to be a major structure which controlled its tectono-metamorphic/magmatic evolution since the Proterozoic times (Danguene et al. 2014; Mapoka et al. 2010; Nzenti et al. 1988). Clarifying the northward extension of the high-pressure Yaoundé and Nyong–Ogooué series, distinction of the different portions of crust with different age, and localization of the ca.2000 Ma relict

zones on the fold belt is, therefore, needed to understand the orogenic assembly of the North Equatorial Fold Belt in CAR and allow a better understanding of the geodynamic significance of the ca. 2000 Ma relicts to the north of the Archean Congo-Sao Francisco Craton.

The Bossangoa-Bossembélé area characterized by the occurrence of well-exposed granulite facies rocks is a suitable site for studying the metamorphic evolution and their geodynamic significance in the NEFB in CAR. The relative timing of these metamorphic events is still unclear in many parts of the CAR. The field mapping carried out during this present study has revealed excellent exposures of the gneiss and has inspired this contribution. These good exposures of the granulitic unit, spanning a continuous range of chemical compositions (with about 58–82 wt.-% SiO_2), make the Bossangoa-Bossembélé area a key site to study the formation of granulitic rocks in this part of the NEFB. This paper provides new data on the geology and the first SHRIMP U-Pb zircon age of the main representative gneiss and discusses the geological significance and petrogenesis of Paleoproterozoic high-grade rocks from the northern part of the CAR in the NEFB. A comparison of the studied granulite with similar rock types in this region is also provided.

Geological setting

The CAR has been divided into three major structural units (Cornacchia et al. 1989; Rolin 1992; Nzenti 1998). The southern unit represents a northern part of Congo Craton and consists of (i) micaschists and quartzites of Archean and Paleoproterozoic age (Poidevin 1991); (ii) metabasites (amphibolites, pyroxenites of Mbomou) of Archean age (2900 Ma; Lavreau et al. 1990); (iii) charnockites series and gneiss similar to those of the Congo Craton in Cameroon (Pin and Poidevin 1987); and (iv) Archean greenstones (komatiites), itabirites, greywacke, rhyodacitic tuffs, and granitoids (Cornacchia and Giorgi 1989). The study area (Figs. 1 and 2) belongs to the intermediate or central domain and consists of Archean gneisses, metabasites, granites, meta-sedimentary rocks, and migmatites (e.g., Danguene et al. 2014; Mapoka et al. 2010, and references therein). The northern part is composed of granulites, orthogneisses, and granites of Neoproterozoic age (833 ± 66 Ma). It corresponds to the western extension of the Pan-African fold belt in Cameroon.

Analytical methods

Whole-rock geochemistry

After the petrographic investigation of the rock units, 16 representative samples were selected for whole-rock chemical analysis. Samples were crushed and subsequently reduced to a very fine powder by grinding in a tungsten carbide ring mill. Major and trace element concentrations of whole-rock were analyzed by X-ray fluorescence spectrometry and LA-ICP-MS, at the University of Lausanne. Major elements (Si, Ti, Al, Fe, Mn, Mg, Ca, Na, K, P, Cr, and Ni) were measured on fused lithium borate glass disks using a Philips PW2400 X-ray fluorescence spectrometer. Trace elements were measured from pressed powder pellets on the same XRF spectrometer (Nb, Zr, Y, Sr, U, Rb, Th, Pb, Ga, Ni, Cr, V, Ce, Ba, and La), and by LA-ICP-MS on glass disks (Be, Sc, Ti, V, Cr, Ni, Cu, Zn, Y, Zr, Nb, Cs, La, Pr, Nd, Sm, Eu, Gd, Tb, Dy, Ho, Er, Tm, Yb, Lu, Hf, Ta, Pb, Th, and U). Tests were made to assess the amount of trace element contamination, such as Ta and Nb, from the tungsten carbide mill. The samples analyzed in this study are relatively rich in these elements, therefore contamination is considered negligible. Laser ablation measurements were made with a 193-nm Lambda Physik Excimer laser (Geolas 200M system) coupled to a Perkin-Elmer 6100 DRC ICP-MS. Laser settings were 27 kV with a 10 Hz repetition rate, yielding a fluorescence of about 12 J/cm^2 on the ablation site. Helium was used as carrier gas (1.1 l/mn) and NIST612 glass was used as the external standard, and Ca and Al as internal standards (on the basis of electron microprobe measurements on the ablation pit site). BCR2 basaltic glass was regularly used as a monitor to check for reproducibility and accuracy of the system. Results were always within ± 10% range of the values reported by Witt-Eickschen et al. (2003), while Rb, Cs, Y, and especially Cr were sometimes within the ± 10% range of the USGS' recommended values for BCR2. Analytical uncertainties are currently better than 1% for major elements and 5–10% for trace element concentrations higher and lower than 20%, respectively. Analytical precision for rare earth elements (REE) is estimated at 5% when concentrations are >10 times chondritic and at 10% when lower.

Zircon U-Pb geochronology

One sample of sillimanite garnet gneiss (sample 7A) was selected for dating. Two kilograms of the sample was subjected by routine heavy mineral separation. Zircons were hand-picked, mounted in epoxy, and polished. Individual zircon grains were subjected to U-Pb isotopic analysis using the sensitive high-resolution ion microprobe (SHRIMP) at the Research School of Earth Sciences at the Australian National University, Canberra. Detailed SHRIMP analytical procedures have been reported by Compston et al. (1984) and Williams and Claesson (1987). The technique focuses a primary beam of negative oxygen ions in vacuo onto the zircon surface from which a small area (25–30μm diameter) of sputtered positive secondary ions is extracted. Secondary ions, which include Zr, Th, U, and Pb from the zircon, are passed

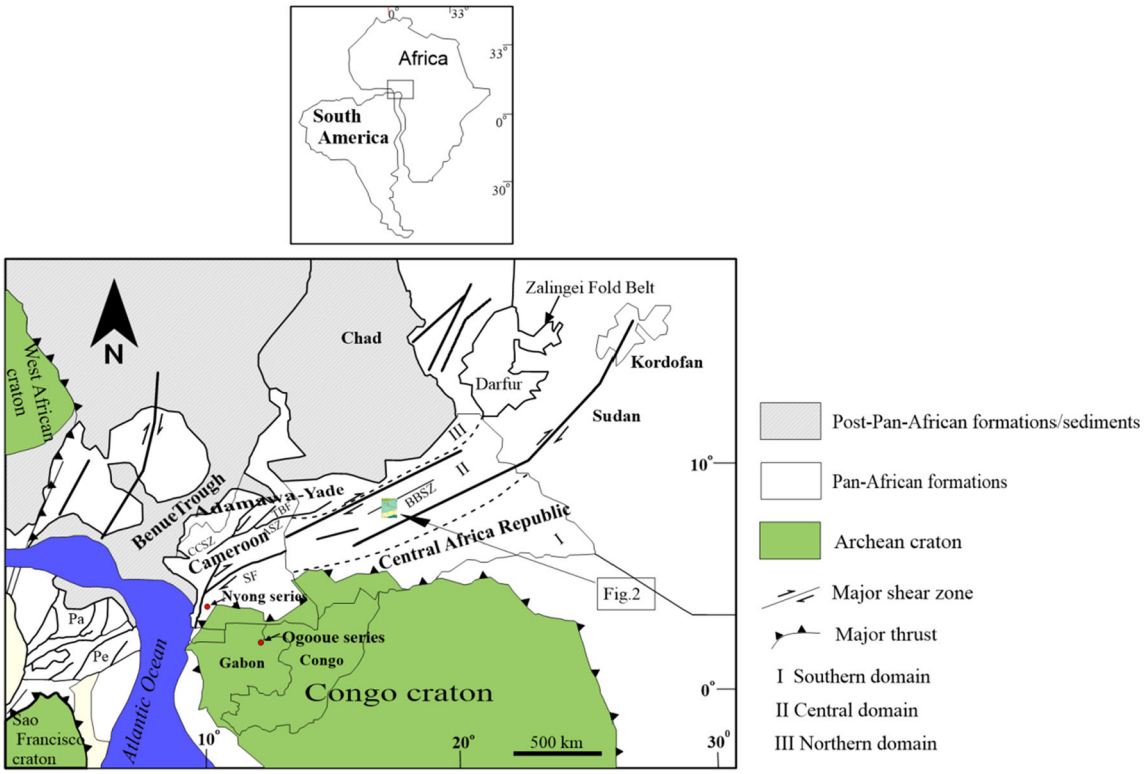

Figure 1 Palinspatic reconstruction of Africa and NE Brazil (Late-Precambrian) modified from Mapoka et al. (2010). ASZ: Adamawa shear zone (or Cameroon Central Shear Zone: CCSZ); SF: Sanaga fault; SL: São Luis Craton; Pa: Patos shear zone; Pe: Pernambuco shear zone; TBF: Tibati-Banyo- Foumban fault. BOF: Bétaré Oya Fault. The study area is marked by a rectangle

through a curvilinear flight path in a strong magnetic field and then counted at a mass resolution of 6500 on a single collector using cyclic magnetic stepping. Isotopic ratios and inter-element fractionation are monitored by continuous reference to a standard Sri Lankan zircon (SL13), fragments of which are mounted with each sample. Progressive changes in the Pb/U ionic ratio during sputtering were corrected using an empirical quadratic relationship between Pb+/U+ and UO+/U+ determined for the standard zircon (Claoue-Long et al. 1995). A radiogenic $^{206}Pb/^{238}U$ ratio of 0.0928 for the standard zircon, corresponding to an age of 572 Ma, is obtained through standard isotope dilution analysis. Initial Pb isotope compositions of the analyzed zircons are assumed to be similar to that of model-derived average crustal Pb of similar age according to Cumming and Richards (1975). The analytical precision of Pb isotope ratios is controlled by machine counting statistics whereas the precision of Pb/U ratios is affected by uncertainties in the recommended Steiger and Jäger (1977) decay constants. Weighted mean $^{207}Pb/^{206}Pb$ ages were obtained for zircons exhibiting an obvious clustering and indistinguishable $^{207}Pb/^{206}Pb$ ages at a 95% confidence level. Individual analyses in the data tables and Concordia diagrams are presented at 1σ. Errors associated with scatter within the cluster are obtained by standard statistical techniques. Dispersion within the cluster is attributed to modern Pb loss.

Results

Petrography and mineral assemblages

The metamorphic rocks are made up of two distinct rock units. The first unit is of sedimentary parentage and mainly composed of pelitic granulites and the second of igneous origin is made up of mafic granulites. All these rocks outcrop as flagstones, lenses, boulders, or boudins (Fig. 3). Granoblastic microstructures prevail in all rock types, although flaser and mylonitic textures are also commonly observed.

Pelitic granulites are predominantly composed of sillimanite bearing garnet gneiss and minor garnet gneiss. They are medium-to coarse-grained layered rocks with alternating millimeter- to centimeter-thick alumina-rich and quartzo-feldspathic layers (Fig. 4a). Garnet frequently shows corona textures with plagioclase, quartz, and biotite rim. They are composed of quartz (20–30%), perthitic K-feldspar (15–20%), plagioclase An_{30-40} (25–30%) occasionally antiperthitic, garnet porphyroblasts (15–20%), biotite (5–10%), and sillimanite (4–8%). Accessory minerals are rutile, zircon, apatite, and graphite. Quartz forms either platy crystals or is in inclusion to garnet and sometimes in pressure shadow of porphyroblasts. Almond shape K-feldspar (5.2 × 3.8 to 6.2 × 3.8 mm) contains opaque minerals. Porphyroblastic garnet crystals (0.4 × 0.24 to 4.4 × 1.7 mm) show the pressure shadow zones filled by quartz, biotite, and sillimanite (Fig. 4a).

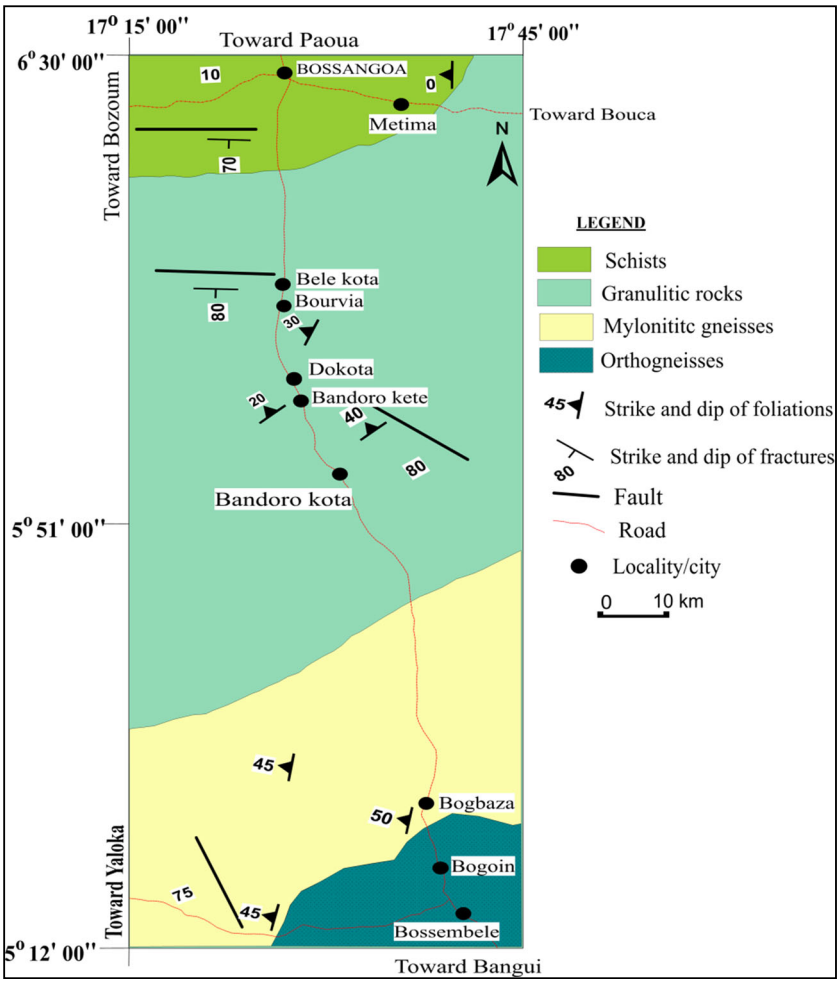

Fig. 2 Geological map of the Bossangoa-Bossembélé area

Fig. 3 Field occurrences of the pelitic granulites and mafic granulites. Flagstones (**a**) and boulder outcrops of pelitic granulites. Flagstones (**c**) and boudins (**d**) of mafic granulites

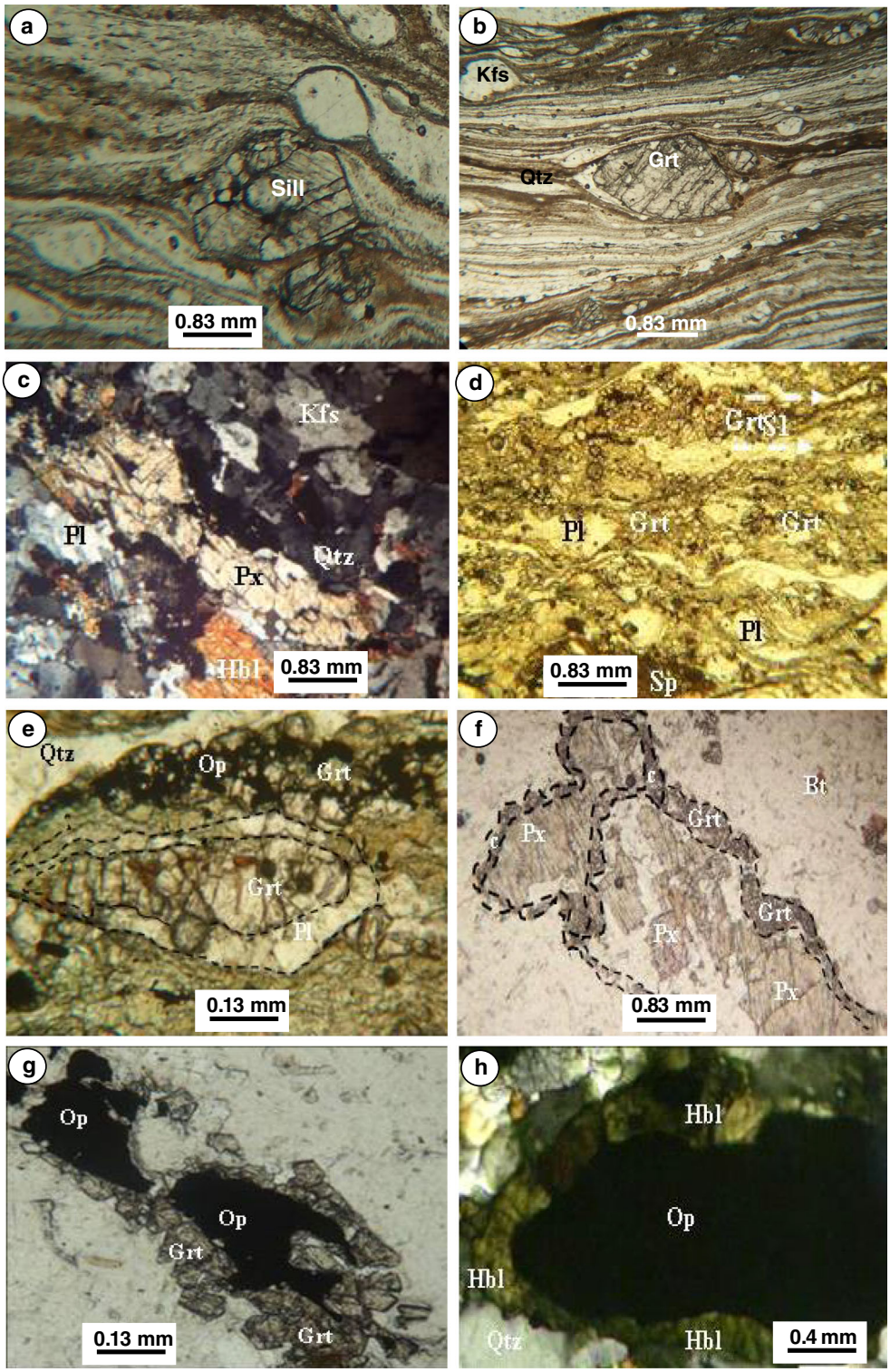

Fig. 4 Photomicrographs of the pelitic granulites and mafic granulites. **a** Porphyroblastic garnet crystals show the pressure shadow zones filled by quartz, biotite, and sillimanite; **b** prismatic crystals of sillimanite molded by mylonitic schistosity; **c** granoblastic microstructure of pyroxene gneiss; **d** composition of gneiss with pyroxene and garnet relicts; **e** kelyphitic rims of garnet composed of amphibole, apatite, quartz, and plagioclase. **f** Pyroxene crystals showing coronitic microstructure; **g**, **h** oxides crystals showing reactional coronas with garnet and hornblende

Prismatic crystals of sillimanite (0.36 × 0.15 to 1.4 × 0.6 mm) are molded by mylonitic schistosity or disseminated on the rock (Fig. 4b). Oxides are included in the garnet porphyroblasts; the smaller ones are oriented elongated. Mineral assemblages are Qtz - Sil - Kfs - Grt - Ru (mineral abbreviations according to Kretz 1983).

The mafic granulites are composed of garnet-pyroxene gneiss associated with gneiss with pyroxene and garnet relicts. These rocks occur mainly as a large flagstone (0.1 to 4 km) along M'poko River, in Bourouma village, but they also occur as boudins within the meta-sedimentary unit (Fig. 3c, d). The mafic granulites are fine- to medium-grained, dark-colored,

and granoblastic and display centimeter-thick alternating quartz-plagioclase and pyroxene-garnet ± biotite layers (Fig. 4c and d). It is composed of quartz (5–15%), clinopyroxene (40–50%), plagioclase (20–30%), almandine garnet (8–10%), and biotite (≥ 5%). Accessory minerals include apatite and oxides (Fig. 4g and h). These rocks show abundant retrograde poikiloblastic hornblende (20–30%) replacing pyroxene whereas some samples contain a significant proportion of titanite and oxides. Quartz forms either oriented platy crystals or small rounded ones (0.1–0.4 mm in diameter). Plagioclase grains are large sub-euhedral crystals (2–5mm) which show granulation. The clinopyroxene (augite in composition) crystals are large (2–6 mm), often zoned, and intensively transformed to green hornblende. Garnet (Fig. 4e) crystals are unzoned with a grain size that varies between 1 and 3 mm. The garnets are almandine type and associated with quartz and clinopyroxene. Orthopyroxene crystals (0.48 × 0.44 to 0.4 × 0.68 mm) display corona with single Qtz - Kfs - Grt rim or double rims (i) Qtz - Kfs - Grt and (ii) Grt - Kfs - Qtz (Fig. 4f). Flakes of biotite occur as secondary minerals in the rock matrix. Primary and secondary mineral assemblages are Qtz - Cpx - Pl - Grt (granulite facies) and Hbl - Bt -Qtz - Spn (amphibolite facies), respectively. The peak metamorphic mineral assemblages identified in the studied mafic granulites are Cpx - Opx - Grt - Qtz - Pl - Op.

Temperature and pressure were estimated from the various mineral assemblages using the mafic granulitic and KFMASH petrogenetic grid (Fig. 5) of Osanai et al. (2006) and Spear et al. (1999), respectively. The average *P-T* conditions of the peak granulite grade metamorphism are ca. 800°C, 10 Kbar (mafic granulites, Fig. 5a), and 7–9 Kbar, 750–800°C (pelitic granulites, Fig. 5b), consistent with temperatures defined from mineral phase assemblages.

Geochemistry

Sixteen representative samples (10 meta-sediments and 6 meta-igneous) were selected for chemical analysis and their whole-rock compositions are listed in Tables 1 and 2.

Pelitic granulites

Meta-sedimentary rocks display the features of pelitic rocks with Fe_2O_3, K_2O, MgO, and TiO_2 closely correlated to Al_2O_3 (Fig. 6a, c, e). All these elements are anticorrelated with silica (Fig. 6b, d, f) suggesting that the protolith of the studied rocks was composed of a quartz-clay mixture. The TiO_2 contents (0.62–0.79%) and TiO_2/Al_2O_3 ratios (0.04–0.11) are high with respect to those of clay (0.04; Goldschimidt 1954; 0.03–0.05; Taylor and McLennan 1985), but correspond to values given for continental terrigene sediments (Van de Camp et al. 1976). The trace element contents (Table 1) are similar to those of shale except for Rb and Sr (Table 1). The Nb contents (1.30–4.04 ppm, average = 1.99 ppm) are low and show a significant variation. This average is very low compared to those of shales (Van de Camp et al. 1976). However, the K/Rb ratios range between 0.01 and 0.04 (average of 0.03), similar to those of the Yaoundé (Nzenti et al. 1988) and Santa Ynez (Van de Camp et al. 1976) meta-sediments. This ratio is slightly higher than that of the upper crust (Taylor and McLennan 1981). Their REE patterns (normalized to chondrite of Evensen et al. 1978) are fractionated, with a slight LREE depletion (Ce_N/Sm_N = 0.9–1.36), flat HREE (Gd_N/Yb_N = 1–1.29), and a strong positive Eu (Eu/Eu*= 4.35–18.59) anomalies (Fig. 7).

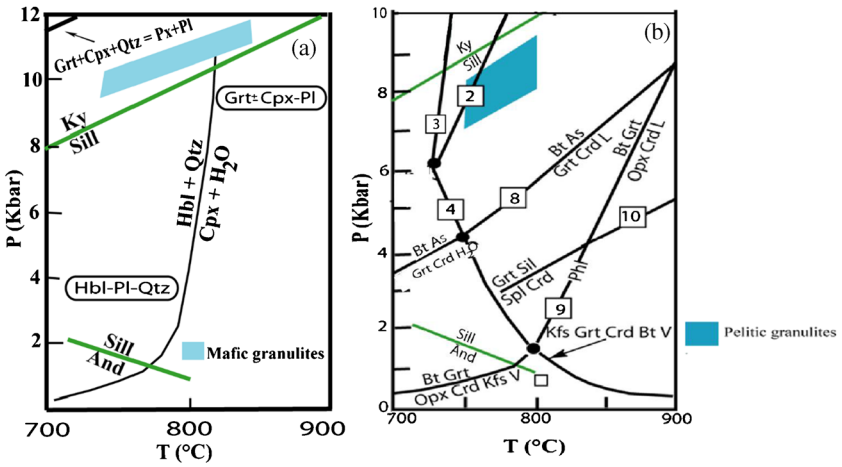

Fig. 5 Synthetic P-T diagrams for the Bossangoa-Bossembele area granulites. Mafic granulites grid (**a**); pelitic granulites in the KFMASH grid (**b**). Hornblende producing univariant reactions are from Spear (1993). Stability of Al-silicates from Holdaway (1971). Stability curves from Berman (1988) and Spear and Cheney (1989) with melting reactions from Vielzeuf and Clemens (1992). (2) Muscovite + quartz + Al_2SiO_5 = K-feldspar + liquid; (3): Muscovite + quartz + H_2O = Al_2SiO_5 + liquid; (4) K-feldspar + Al_2SiO_5 + quartz = H_2O + liquid; (8) Biotite + Al_2SiO_5 + quartz + garnet = cordierite + K-feldspar + liquid; (9) Biotite + garnet + quartz + cordierite = orthopyroxene + K-feldspar + liquid; (10) Garnet + sillimanite + spinel = cordierite + quartz

Table 1 Major (wt%) and trace (ppm) elements compositions for representative pelitic granulite samples from Bossangoa-Bossembélé area

Samples	TCH1DA	7A	TCH1FA	TCH1FB	7A1	TCH1IB	TCH1BA	TCH1BB	TCH1BC	TCH1BD
SiO_2	73.71	73.18	74.55	74.58	82.18	81.87	62.10	69.65	69.89	69.97
TiO_2	0.77	0.79	0.78	0.78	0.62	0.62	1.33	0.63	0.64	0.64
Al_2O_3	12.20	12.37	11.52	11.50	7.07	7.12	12.60	14.41	14.56	14.59
Fe_2O_3	5.07	5.11	4.51	4.49	6.03	6.07	10.07	4.45	4.47	4.46
MnO	0.05	0.05	0.06	0.06	0.11	0.11	0.11	0.04	0.04	0.04
MgO	2.04	2.05	1.82	1.80	1.99	2.00	6.03	2.08	2.08	2.08
CaO	0.26	0.27	0.87	0.87	0.19	0.20	1.52	0.93	0.94	0.93
Na_2O	0.31	0.30	1.05	1.05	0.14	0.18	0.07	3.64	3.59	3.65
K_2O	3.67	3.71	2.58	2.57	0.88	0.91	1.41	1.60	1.59	1.58
P_2O_5	0.03	0.03	0.03	0.03	0.04	0.04	0.20	0.14	0.14	0.14
LOI	1.89	1.82	2.29	2.25	0.88	0.92	4.32	2.11	2.11	2.13
Total	100.01	99.67	100.06	99.97	100.12	100.05	99.75	99.67	100.05	100.21
Ba	838.2	793.4	26.9	28.6	41.0	14.4	176.6	905.8	900.9	876.6
Cr	314.9	298.3	91.4	92.0	217.0	61.7	542.0	470.6	382.5	382.2
Co	383.0	353.0	9.4	9.3	36.6	11.4	249.2	78.7	79.7	75.2
Cu	886.3	585.7	21.0	23.3	77.6	29.0	1329.9	710.9	1052.6	808.4
Ga	1219.7	1074.7	34.2	34.1	51.2	17.3	302.3	529.6	470.1	495.7
Mo	18.7	15.9	0.4	0.3	0.8	0.2	1.3	2.3	2.3	2.1
Nb	3.8	3.9	1.3	1.3	4.0	1.3	28.2	37.1	35.0	33.0
Ni	109.8	89.8	20.3	21.9	71.9	23.8	231.4	132.8	131.5	143.4
Rb	909.7	830.5	74.1	76.0	131.1	24.8	753.4	3008.3	2943.4	2915.0
Sc	52.0	48.0	16.8	17.5	49.4	14.4	148.5	114.3	107.3	107.9
Sr	840	779	25	25	102	33	244	250	245	240
V	353.1	333.8	102.8	104.3	218.3	67.0	928.8	676.9	647.2	659.1
W	167.8	147.2	7.8	8.2	23.2	6.9	34.2	98.2	101.8	137.8
Y	870	802	278	270	779	263	173	339	336	328
Zn	247.0	231.6	68.1	66.7	323.5	109.9	148.0	99.5	97.3	98.6
Zr	387.5	357.2	12.7	13.1	63.3	18.9	87.4	82.4	81.0	78.1
La	20.87	20.02	21.63	21.11	21.45	20.41	21.36	21.56	20.88	20.10
Ce	35.26	28.45	27.58	26.16	28.19	25.64	25.17	27.20	27.00	26.72
Pr	3.95	3.30	3.59	2.69	2.77	2.64	2.89	2.61	2.12	2.46
Nd	14.46	11.16	9.75	9.82	10.07	8.65	7.66	8.74	8.40	7.54
Sm	3.90	3.51	1.08	1.06	2.32	0.79	1.00	2.09	2.12	1.90
Eu	13.73	13.25	4.13	4.14	15.15	4.97	3.94	5.85	5.87	5.76
Gd	22.76	19.42	0.59	0.69	2.71	0.97	6.77	8.17	8.10	7.86
Tb	15.6	13.9	4.3	4.4	17.8	6.1	4.6	4.8	5.1	4.9
Dy	20.51	20.43	10.16	8.07	8.33	7.90	7.67	8.00	7.66	7.23
Ho	9.1	8.7	2.6	2.7	11.3	3.6	2.6	2.8	2.7	2.6
Er	13.58	14.29	5.37	4.95	4.07	5.06	6.28	4.07	6.22	5.90
Tm	1.87	1.99	0.67	0.75	0.73	0.73	0.72	0.70	0.71	0.77
Yb	11.02	13.63	5.31	5.34	5.61	5.90	4.72	6.26	6.16	6.26
Lu	1.75	1.66	1.49	1.17	1.55	1.30	1.28	1.39	1.62	1.40
Y/Nb	229	207	210	208	193	199	6	9	10	10
$(La/Yb)_N$	1.27	0.99	2.73	2.65	2.57	2.32	3.03	2.31	2.28	2.15
$(Gd/Yb)_N$	1.65	1.14	0.09	0.10	0.38	0.13	1.14	1.04	1.05	1.00
$(Ce/Sm)_N$	2.12	1.90	6.01	5.78	2.86	7.58	5.91	3.05	2.98	3.29
Eu/Eu*	4.48	4.94	15.90	14.89	18.59	17.37	4.65	4.35	4.35	4.58

Table 2 Major (wt%) and trace (ppm) elements data for representative mafic granulite samples from Bossangoa-Bossembélé area

Samples	LERE2A	LERE2B	LERE2A2	LERE1B	bgna1B	bgna1C
SiO_2	59.19	59.03	58.04	59.41	56.48	56.21
TiO_2	1.38	1.39	1.32	1.26	1.26	1.26
Al_2O_3	17.16	17.18	17.75	17.55	16.53	16.49
Fe_2O_3	8.26	8.25	7.91	7.58	7.94	7.97
FeO*	7.44	7.43	7.12	6.82	7.15	7.18
MnO	0.14	0.14	0.13	0.13	0.15	0.14
MgO	3.09	3.10	3.12	2.95	3.87	3.88
CaO	5.15	5.14	6.34	5.69	6.89	6.92
Na_2O	2.72	2.73	3.39	3.00	3.96	3.98
K_2O	2.50	2.48	1.59	2.26	1.91	1.88
P_2O_5	0.35	0.34	0.36	0.31	0.33	0.34
LOI	0.31	0.35	0.17	0.01	0.82	0.84
Total	100.25	100.13	100.12	100.15	100.13	99.90
Ba	197.2	250.2	1098.1	12.74	715.1	177.5
Be	2.6	1.6	3.9	3.67	3.3	1.2
Cr	109.3	1450.4	95.3	0.02	1415.7	1268.9
Co	24.0	73.8	59.5	3.94	58.6	114.9
Cu	74.1	43.0	323.1	17.84	217.9	109.1
Ga	18.1	26.6	54.6	8.30	41.1	17.7
Mo	25.4	1.3	0.8	184.78	0.5	0.6
Nb	10.3	3.3	44.0	0.15	11.0	8.0
Ni	70.4	466.6	60.5	2.47	402.1	1109.8
Rb	27.3	10.5	96.8	2.30	73.2	5.1
Sc	17.5	39.8	49.4	17.98	35.8	37.5
Sr	344	182	339	52	187	153
V	123.1	221.2	545.3	12.89	241.1	321.4
W	1.8	0.2	0.4	0.14	0.4	0.1
Y	27	22	60	2	28	18
Zn	83.1	129.9	186.9	9.93	205.3	157.2
Zr	136.8	42.1	341.4	0.26	225.6	67.5
La	28.1	15.7	46.8	1.42	54.1	13.9
Ce	59.6	36.4	104.0	5.75	144.4	40.8
Nd	26.7	15.7	55.8	0.33	78.6	25.0
Sm	5.2	3.4	11.7	0.77	13.4	5.7
Eu	1.1	0.8	3.4	0.09	3.0	1.4
Gd	4.9	3.8	12.4	0.51	9.6	4.7
Tb	0.7	0.6	1.9	0.09	1.1	0.6
Dy	4.7	3.9	11.8	0.22	5.7	3.7
Er	2.8	2.5	6.3	0.20	2.4	1.7
Yb	2.8	2.2	5.9	1.19	2.1	1.6
Lu	0.4	0.3	0.8	0.09	0.3	0.2
Y/Nb	2.6	6.8	1.4	17.0	2.5	2.2
$(La/Yb)_N$	6.82	4.86	5.35	0.80	17.07	5.88
$(Gd/Yb)_N$	1.41	1.42	1.68	0.34	3.59	2.36
$(Ce/Sm)_N$	2.68	2.49	2.09	1.76	2.54	1.67
Eu/Eu*	0.67	0.72	0.86	0.44	0.82	0.80

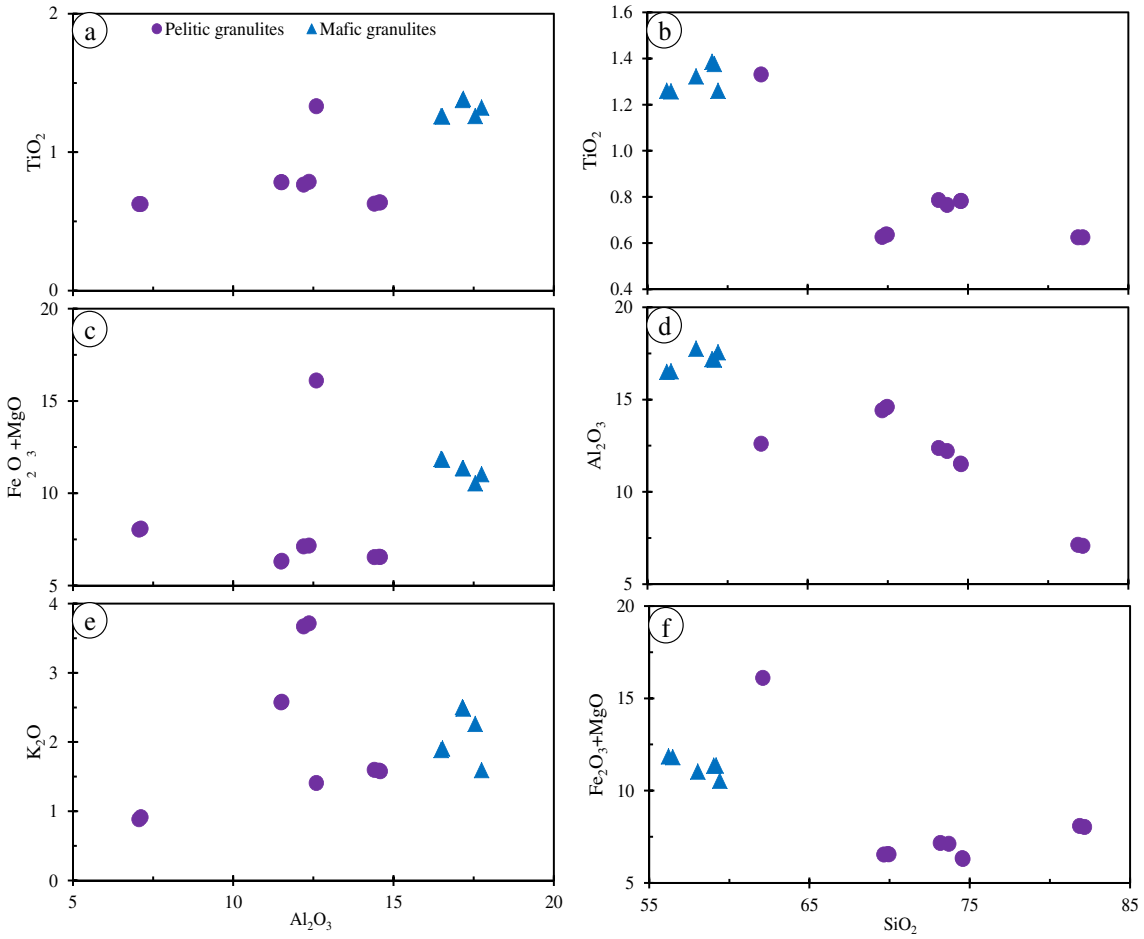

Fig. 6 Binary plots of some major elements (versus Al_2O_3 and SiO_2) for pelitic granulites

Mafic granulites

Meta-igneous rocks have the composition of diorite (Table 2) with a silica content ranging from 58.04 to 61.71 wt% respectively and rather constant alumina content (17.16 to 17.75 wt %). They are enriched in Al_2O_3, Fe_2O_3, MgO, Ba, and Rb (except sample LERE2B). TiO_2 contents and FeO*/MgO ratios vary from 1.1 to 1.39 wt% and 2.26–2.41 respectively. The iron enrichment with the values of titanium in these rocks is comparable to those of the tholeiitic series. Also, CaO/TiO_2 (3.71–4.52) and Al_2O_3/TiO_2 (>12) ratios correspond closely to those of oceanic tholeiites (Shibata et al. 1979; Leeman et al. 1980). The investigated samples are enriched in alkalis ($4.98 \leq Na_2O + K_2O \leq 5.21\%$), and CaO (5.14–6.34%). Compared to the gabbros described by Le Maître (1976), they have similar contents of major elements. Ba (197–1098 ppm),

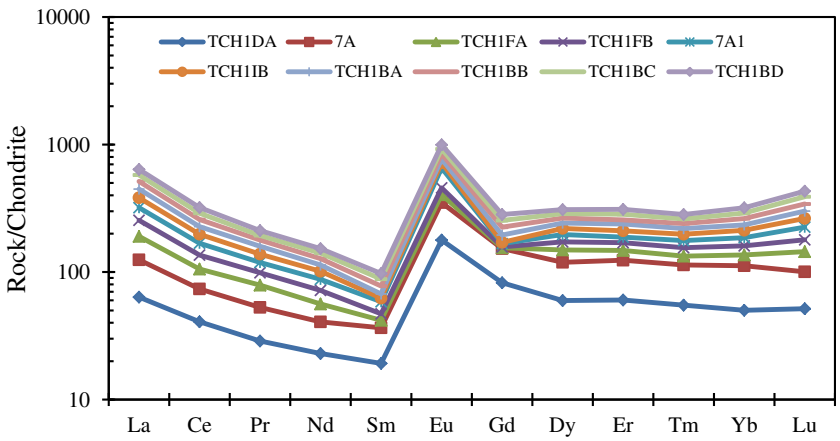

Fig. 7 Chondrite-normalized REE patterns of pelitic granulites

Sr (182–344 ppm), Cr (95–1450 ppm), and Ni (60–467ppm) contents are variable and high while those of Nb (3 to 44 ppm), Rb (10–97 ppm), Y (22–60 ppm), Zn (83–187 ppm), and Zr (42–341 ppm) are variable and relatively low. The high contents of Cr, Ni, Sr, and Y are probably related to the fractionation of pyroxene and garnet. The binary element diagrams of some major elements versus MgO (Fig. 8a–f) show that these rocks have the same evolutionary tendency characterized by the decrease of SiO_2 and a positive correlation in CaO, TiO_2, Fe_2O_3, and P_2O_5. The Y/Nb ratios > 1 are similar to those of tholeiites (Pearce and Cann 1973). Plotting in the TiO_2 vs. FeO*/MgO diagram (Miyashiro 1974; Fig. 9a), all these rocks fall in the tholeiites field. Their REE patterns (Figure 9b) are fractionated (La_N/Yb_N = 4.82–359.13); LREE enrichment (Ce_N/Sm_N = 1.76–2.68 and Gd_N/Yb_N = 0.34–1.68) relative to HREE, and show a negative Eu anomaly (Eu/Eu* = 0.44 to 0.82). These behaviors are intermediary between continental and oceanic tholeiites (Shibata et al. 1979; Leeman et al. 1980). Their overall trace element patterns (Fig. 9c) show Th, Nb, Sr, Zr, and Y anomaly, suggesting the participation of the continental crust and mantle in their genesis (Thompson et al. 1984).

SHRIMP U-Pb zircon age

The zircons from the study sample 7A show a wide range of shapes, sizes, and colors (Fig. 10). A dominant form, however, is the near-spherical, clear, "soccerball" type usually formed during high-T metamorphism (Vavra et al. 1996, 1999; Schaltegger et al. 1999; Hoskin and Black 2000; Kelly and Harley 2005). The grains show a variety of internal structures, included inherited cores, and no oscillatory zoning. The rounded soccer ball/metamorphic zircons are generally dark in CL and show limited zoning. All types and generations of zircon were analyzed (Table 3). The multifaceted to rounded forms with their wide external zones, poorer in uranium, suggest a metamorphic growth type (Pidgeon 1992; Kelly and Harley 2005). The Th/U ratios vary from 0.72 to 0.82 in the

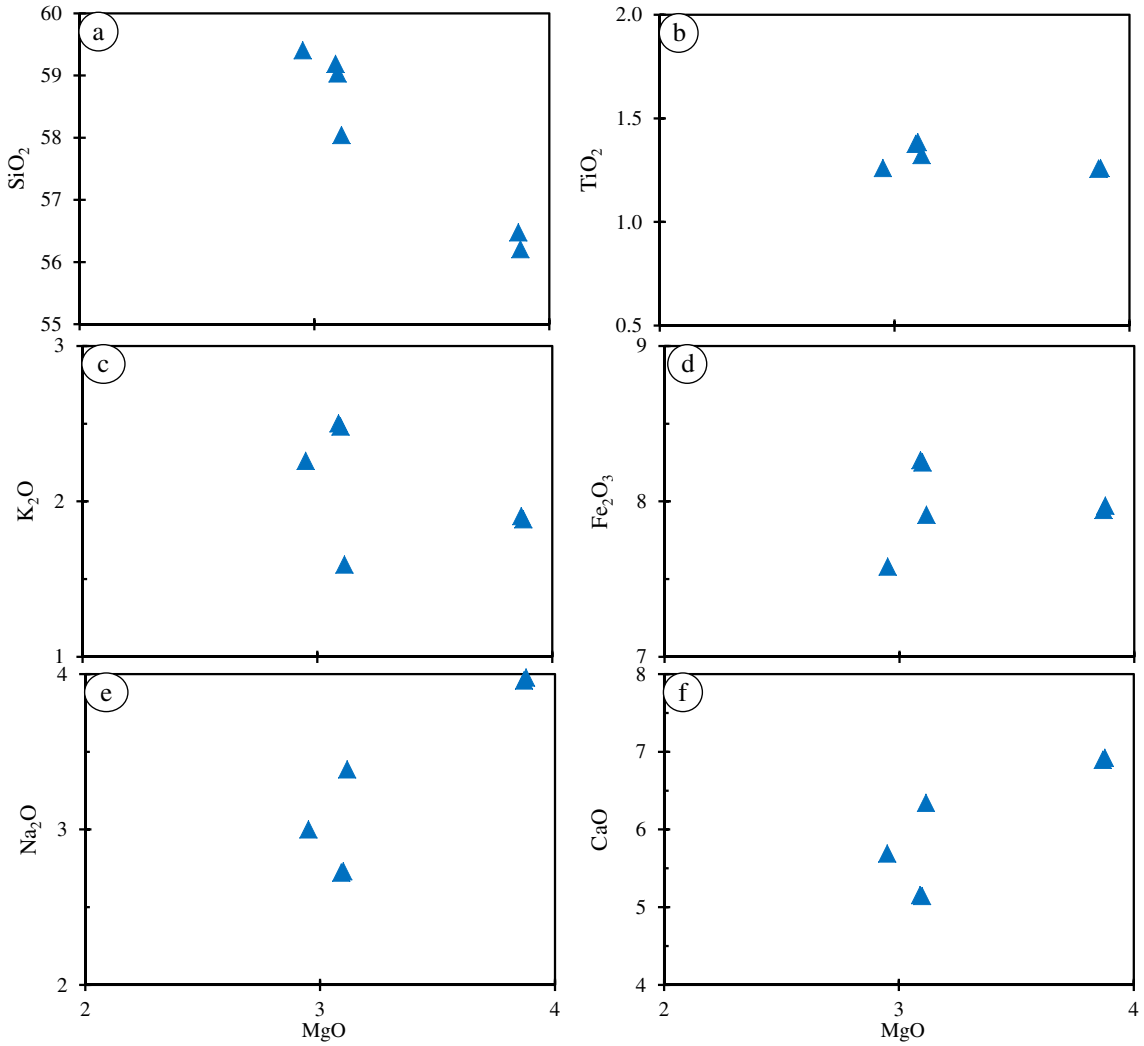

Fig. 8 Binary diagrams of some major elements versus MgO of mafic granulites

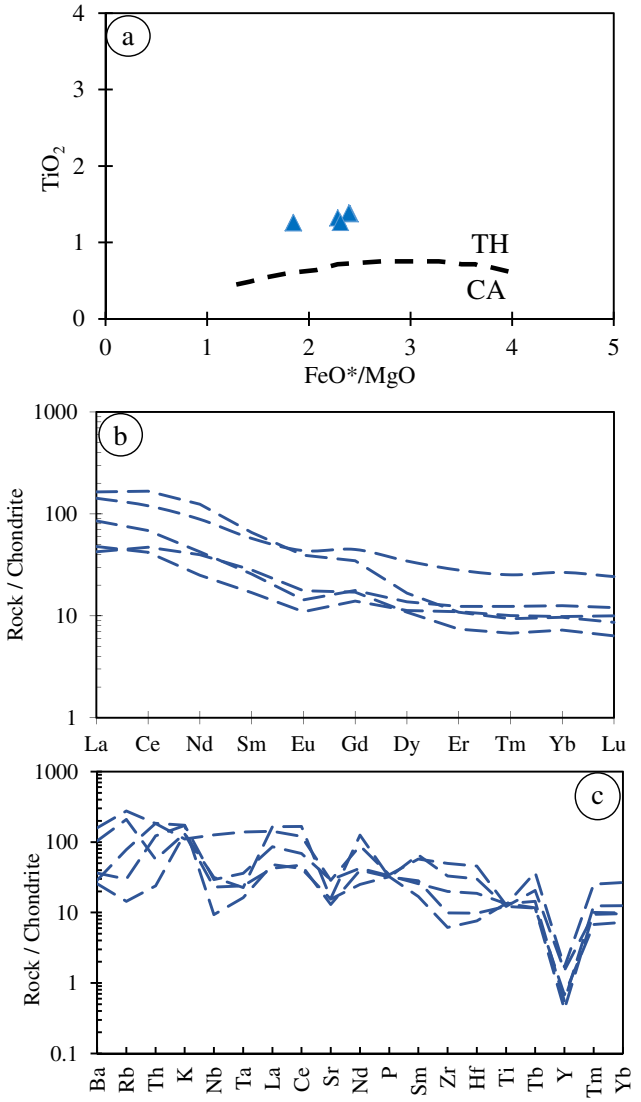

Fig. 9 **a** TiO_2 vs. FeO*/MgO diagram; **b** REE patterns of mafic granulites; **c** multi-element patterns of mafic granulites

core to 0.08 to 0.19 in the external zone (Table 2). On the Concordia diagram (Fig. 11), the older zircon fractions yielded an upper intercept age of 1952 Ma, younger ones cluster on Concordia to give a weighted mean $^{206}Pb/^{238}U$ age of 640.8 ± 6.0 Ma.

Discussion

The Bossangoa-Bossembélé area consists of both pelitic and mafic granulites. The pelitic granulites are derived from pelite and greywacke, while the mafic granulites display the chemical composition of intermediate to basic tholeiitic rocks. Petrography and mineral assemblages (Grt-Cpx-Pl-Qtz and Grt-Pl-Sill-Qtz) indicate peak metamorphic conditions under granulite facies at about 800°C, 10 Kbar (mafic granulites) and 8 kbar (pelitic granulites). From the CL imaging, the zircon grains extracted from the pelitic granulites display either no sector or planar zoned which are commonly attributed to high-T subsolidus growth and melt crystallization growth, respectively (Pidgeon 1992; Schaltegger et al. 1999; Ashwal et al. 1999; Hoskin and Black 2000; Corfu et al. 2003; Kelly and Harley 2005). In addition, complete transgression of older zones by sharp fronts or visible compositional zones were not observed on these zircons suggesting that in situ modification under high-T conditions can be ruled out. Furthermore, even partial modification commonly expressed by "ghost-like" or "bleached" for former oscillatory zones was noticed as all the zircons are blurred (e.g., Corfu et al. 1994; Vavra et al. 1996, 1999; Harley et al. 2001, 2007; Carson et al. 2002). These observations suggest that the studied zircon grains were not formed as the result of a high-T anatectic melt growth or late-stage mineral-fluid interactions at temperatures well below those of the high-T metamorphic event.

Based on the morphology and structure of zircons, the peak metamorphic mineral assemblages probably correspond to a pre-Pan-African H*P*-H*T* metamorphic cycle. Indeed, phase

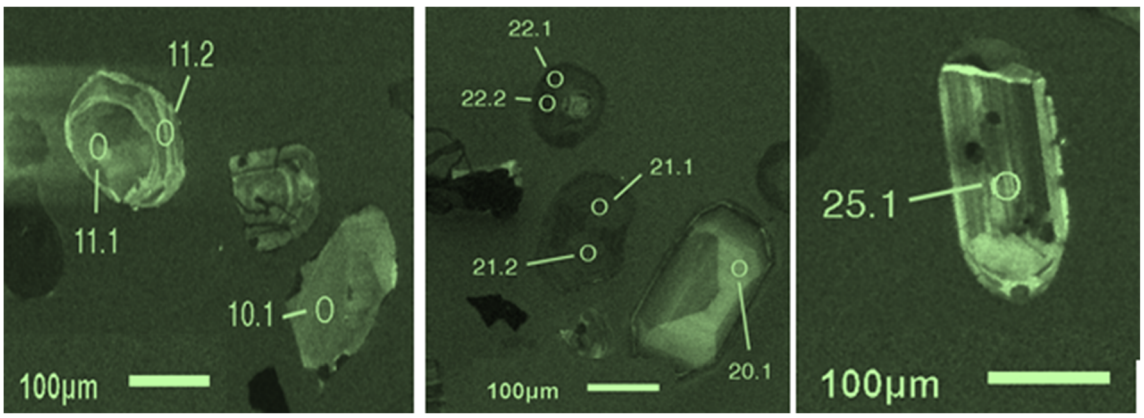

Fig. 10 Cathodoluminescence (CL) images of typical zircons from the pelitic granulites (7A). Note the near-spherical, clear, "soccerball" type usually formed during metamorphism. The grains show a variety of internal structures, included inherited cores and no oscillatory zoning, no sector- or planar zoned, no "ghost-like" or "bleached" for former oscillatory zones

Table 3 SHRIMP U-Pb zircon data for the selected sample (7A) of the Bossangoa-Bossembélé pelitic granulites

Grain spots	Trace elements content (ppm)					Isotopic ratios							Ages (Ma)				Dis.
	% ^{206}Pbc	^{206}Pb*	Th	U	Th/U	^{207}Pb*/^{206}Pb	±1s	^{207}Pb*/^{235}U	±1s	^{206}Pb*/^{238}U	±1s	err corr	(1) ^{207}Pb/^{206}Pb	±1s	(1) ^{206}Pb/^{238}U	±1s	%
1.1	0.00	13.2	40	98	0.42	0.0711	1.8	1.539	2.3	0.1569	1.4	.633	961	36	940	13	2
2.1	0.00	38.1	68	417	0.17	0.06135	0.86	0.899	1.4	0.1063	1.1	.790	652	18	651.3	6.9	0
3.1	0.07	53.1	31	578	0.06	0.06281	0.78	0.926	1.3	0.107	1.1	.813	702	17	655.2	6.7	7
4.1	0.00	40.2	82	444	0.19	0.06107	0.84	0.888	1.4	0.1055	1.1	.796	642	18	646.5	6.8	−1
5.1	0.02	61.6	123	287	0.44	0.12429	0.73	4.282	1.6	0.2499	1.4	.887	2019	13	1438	18	29
7.1	--	50.7	298	390	0.79	0.0715	1.4	1.488	1.8	0.151	1.1	.621	971	29	906.6	9.6	7
8.1	0.05	32.2	85	354	0.25	0.06042	1.1	0.882	1.5	0.1059	1.1	.731	618	23	649	7	−5
9.1	0.07	66.7	123	261	0.49	0.1137	5	4.66	5.1	0.2971	1.2	.233	1859	90	1677	18	10
10.1	--	15.4	54	106	0.53	0.0731	1.8	1.713	2.3	0.1699	1.4	.616	1018	36	1012	13	1
11.1	0.00	16.3	80	100	0.82	0.0767	4.9	2	5.1	0.1893	1.4	.284	1114	98	1118	15	0
11.2	0.35	12.7	65	88	0.76	0.0786	3.3	1.8	3.6	0.1661	1.6	.444	1162	64	991	15	15
12.1	0.00	39.2	79	436	0.19	0.06236	0.87	0.899	1.4	0.1046	1.1	.789	686	19	641	6.8	7
14.1	--	24.6	91	185	0.51	0.0721	2.4	1.547	2.8	0.1557	1.3	.462	988	50	933	11	6
15.1	0.07	6.65	34	58	0.61	0.0818	6.8	1.5	7.3	0.1331	2.7	.372	1240	130	805	21	35
16.1	0.02	61.6	83	693	0.12	0.0629	1.6	0.897	2	0.1034	1.2	.575	705	35	634.2	7	10
17.1	--	27.4	59	115	0.53	0.09903	0.86	3.777	2	0.2766	1.9	.908	1606	16	1574	26	2
18.1	--	16.6	61	82	0.77	0.1326	5.2	4.31	5.4	0.236	1.5	.275	2133	92	1366	18	36
19.1	0.00	45.7	47	520	0.09	0.0609	0.8	0.859	1.4	0.1023	1.1	.808	636	17	627.9	.6	1
19.2	0.00	53.8	57	610	0.10	0.06051	0.64	0.858	1.2	0.1028	1.1	.856	622	14	630.8	6.4	−1
20.1	--	12.2	60	87	0.72	0.0763	4.5	1.719	4.8	0.1635	1.5	.317	1102	91	976	14	11
21.1	0.03	141	235	483	0.50	0.1184	2.8	5.56	4.1	0.341	3	.728	1933	51	1890	49	2
22.1	0.00	48.6	53	553	0.10	0.06118	0.84	0.863	1.4	0.1023	1.1	.793	645	18	627.7	6.6	3
22.2	0.00	55.6	51	623	0.08	0.06097	0.64	0.874	1.2	0.1039	1.1	.860	638	14	637.4	6.5	0
23.1	0.03	51.9	87	570	0.16	0.06188	0.75	0.904	1.3	0.1059	1.1	.827	670	16	649	6.8	3
23.2	0.00	41.3	88	458	0.20	0.06089	0.73	0.881	1.3	0.1049	1.1	.829	635	16	643.3	6.6	−1
24.1	0.07	26.4	57	127	0.46	0.104	6	3.46	7.2	0.241	3.9	.538	1697	110	1392	48	18
25.1	0.00	12.1	145	84	1.77	0.0753	1.9	1.742	3	0.1678	2.3	.767	1077	39	1000	21	7

Errors are 1-sigma; Pb_c and Pb^* indicate the common and radiogenic portions, respectively

Error in standard calibration was 0.32% (not included in above errors but required when comparing data from different mounts)

(1) Common Pb corrected using measured ^{204}Pb

assemblages indicate that the conditions of metamorphism culminated during Paleoproterozoic time as revealed by the U-Pb zircon core upper intercept age of ca 1952 Ma. These rocks which have also suffered Pan-African orogeny at 640.8 ± 6.0 Ma form a polycyclic unit with a complex evolution corresponding to Paleoproterozoic H*P*-H*T* metamorphic cycle followed by Pan-African M*P*-M*T* tectono-metamorphic event. The older age (1952 Ma) is interpreted to represent the age of crystallization of the zircons during granulite metamorphic conditions. The younger age (640 Ma) corresponds to a younger Pan-African tectono-metamorphic event. The frequency of high-pressure granulite facies assemblages indicates that the base of the crust was reworked during the Pan-African orogeny. The H*P*-H*T* conditions during or close to peak metamorphic conditions are in accordance with previous studies in other Paleoproterozoic areas in the Pan-African fold belt in Cameroon (Tanko Njiosseu et al. 2005; Nzenti et al. 2007; Ganwa et al. 2008, 2011; Ndema Mbongue et al. 2014), suggesting that the whole central part of the belt which is presently exposed represents the same crustal level. The new findings suggest that a Paleoproterozoic continental crust was involved in the Pan-African North Equatorial fold belt from the south (Nyong and Ogooué series) to the north. In addition, strong similarities (granulitic rocks with similar composition and ages) exist between the studied rocks and high-grade gneisses of eastern Nigeria (Dada et al. 1989) and of the Transamazonian belt of NE Brazil (Van Schmus et al. 1999; Brito Neves et al. 2002; Neves et al. 2006). This implies that the Pan-African sedimentary series were deposited on an old Paleoproterozoic continental crust extending up to the north, in CAR, Chad, and Sudan. Thus the Bossangoa-Bossembélé and Nyong and Ogooué series are the extensions in central Africa of the Transamazonian belt.

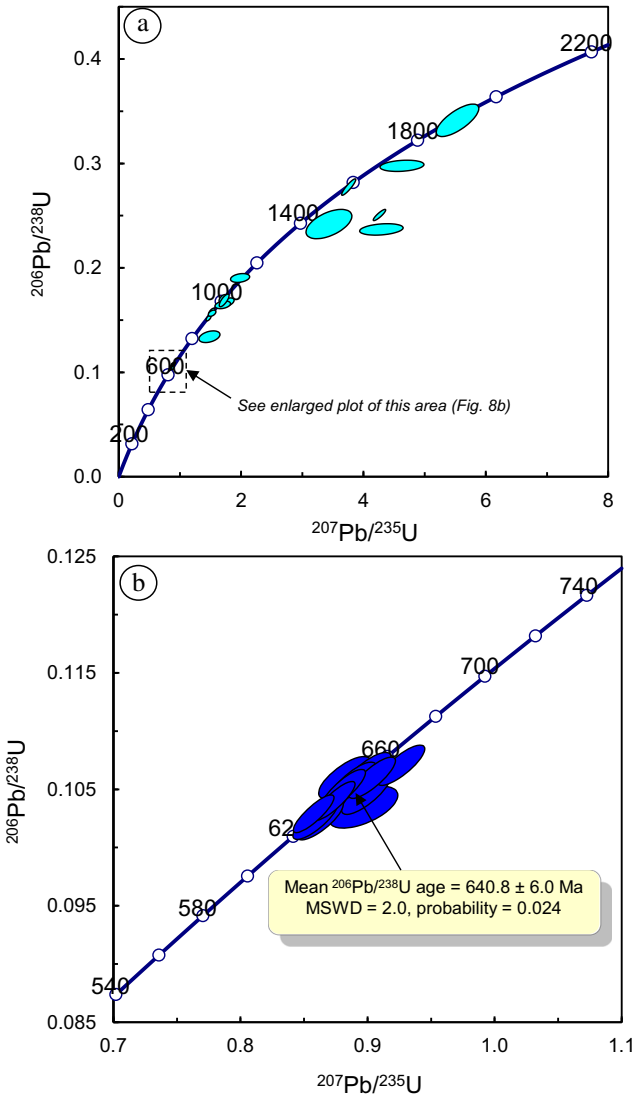

Fig. 11 Concordia diagram showing all SHRIMP data points for old (**a**) and younger (**b**) zircon grains from the pelitic granulites (sample 7A)

Conclusion

The petrographic and geochronological investigations of the Bossangoa-Bossembélé area have led to the following conclusions:

1. The Bossangoa-Bossembélé consists of both pelitic and mafic granulites. The pelitic granulites were derived from pelite and greywacke, while the mafic granulites display the chemical composition of diorite.
2. The peak metamorphic conditions are indicated by Cpx - Opx - Grt - Qtz - Pl and Grt -Pl - Sill - Qtz granulitic mineral assemblages.
3. SHRIMP U-Pb zircon dating results indicated that the peak H*P*-H*T* metamorphic conditions were reached during the Eburnean/Transamazonian orogeny at ca. 1952 Ma. The studied rocks which were later affected by the Pan-African orogeny at 640.8 ± 6.0 Ma form a polycyclic unit with a complex evolution corresponding to Paleoproterozoic HP-HT metamorphic cycle followed by Pan-African MP-MT tectono-metamorphic event.
4. The Congo craton spreads not only far from the southern part of the North Equatorial fold belt in Cameroon as initially suggested but on the whole fold belt from south to the north (CAR, Chad, Sudan).
5. The Bossangoa-Bossembélé and Nyong and Ogooué series are the extensions in central Africa of the Transamazonian belt.

Acknowledgements The authors are grateful to Prof. Roberto Braga and Prof. Faouziya Haissen for their thorough comments, which have greatly improved the manuscript.

Funding The authors received financial support from SCAC (Service de la Coopération et d'Action Culturelle) Bangui and support from Professor Richard Armstrong of the National University of Canberra (Australia).

Declarations

Conflict of interest The authors declare no competing interests.

References

Ashwal LD, Tucker RD, Zinner EK (1999) Slow cooling of deep crustal granulites and Pb-loss in zircon. Geochim Cosmochim Acta 63: 2839–2851

Berman RG (1988) Internally consistent thermodynamic data for minerals in the system Na_2O-K_2O-CaO-MgO-FeO-Fe_2O_3-Al_2O_3-SiO_2-TiO_2-H_2O-CO_2. J Petrol 29:445–522

Brito Neves BB, Van Schmus WR, Fetter A (2002) North-western Africa-North eastern Brazil: major tectonic links and correlation problems. J Afr Earth Sci 34:275–278

Carson CJ, Ague JJ, Grove M, Coath CD, Harrison TM (2002) U–Pb isotopic behaviour of zircon during upper-amphibolite facies fluid infiltration in the Napier Complex, east Antarctica. Earth Planet Sci Lett 199:287–310

Claoue-Long JC, Compston W, Roberts J, Fanning CM (1995) Two carboniferous ages: a comparison of SHRIMP zircon dating with conventional zircon ages and 40Ar/39Ar analysis. In: Berggren WA, Kent D, Aubry MP, Hardenbol J (eds) Geochronological time scales and global stratigraphic correlation, Soc. Econ. Paleo. and Mineral Spec. Pub, vol 54, pp 3–21

Compston W, Williams IS, Meyer C (1984) U-Pb geochronology of zircons from lunar breccia 73217 using a sensitive high mass-resolution ion microprobe. J Geophys Res 89:525–534

Corfu F, Heaman LM, Rogers G (1994) Polymetamorphic evolution of the Lewisian complex, NW Scotland, as recorded by U-Pb isotopic compositions of zircon, titanite and rutile. Contrib Mineral Petrol 117:215–228

Corfu F, Hanchar JM, Hoskin PWO, Kinny P (2003) Atlas of zircon textures. In: Hanchar JM, Hoskin PWO (eds) Zircon, Mineralogical Society of America Reviews in Mineralogy & Geochemistry, vol 53, pp 469–495

Cornacchia M, Giorgi L (1989) Discordances majeures et magmatisme des séries précambriennes de la région de Bogoin, Centre Ouest de la République centrafricaine. J Afr Earth Sci 9:221–226

Cornacchia M, Giorgi L, Caruba C, Vivrier G (1989) Existence d'une zone de suture sur la marge Nord du craton congolais (secteur de Bangui, centre de la République centrafricaine). C R Acad Sci Paris 308(2):107–110

Cumming GL, Richards JR (1975) Ore lead isotope ratios in a continuously changing Earth. Earth Planet Sci Lett 28:155–171

Dada SS, Lancelot JR, Briqueu L (1989) Age and origin of the annular charnockites complex at Toro, Northern Nigeria: U-Pb and Rb-Sr evidence. J Afr Earth Sci 9(2):227–234

Danguene PEY, Ngnotue T, Ganno S, Biandja J, Kankeu B, Nzenti JP (2014) Paleoproterozoic synkinematic magnesian high-K magmatism from the Tamkoro-Bossangoa Massif along the Bossangoa-Bossembele Shear Zone in north-western Central African Republic. J Geosci Geomatics 2(4):151–164

Evensen NM, Hamilton P, O'Nions RK (1978) Rare earth abundances in chondritic meteorites. Geochim Cosmochim Acta 4:1199–1212

Ganwa AA, Frisch W, Siebel W, Ekodeck GE, Cosmas SK, Ngako V (2008) Archean inheritances in the pyroxene-amphibole-bearing gneiss of the Méiganga area (Central North Cameroon): Geochemical and 207Pb/206Pb age imprints. C R Géosci 340: 211–222

Ganwa AA, Siebel W, Shang CK, Seguem N, Ekodeck GE (2011) New constraints from Pb-evaporation zircon ages of the Méiganga amphibole-biotite gneiss, Central Cameroon, on Proterozoic crustal evolution. Int J Geosci 2(2):138–147

Goldschimidt HJ (1954) Geochemistry. Clarendon Press

Harley SL, Kinny PD, Snape I, Black LP (2001) Zircon chemistry and the definition of events in Archaean granulite terrains. In: Cassidy KF, Dunphy JM, van Kranendonk MJ (eds) Extended Abstracts of 4th International Archaean Symposium. AGSO-Geoscience Australia Record 2001/37, Canberra, pp 511–513

Harley SL, Kelly NM, Möller A (2007) Zircon behavior and the thermal histories of Mountain chains. Elements 3:25–30

Holdaway MJ (1971) Stability of andalusite and the aluminum silicate phase diagram. Am J Sci 271:97–131

Hoskin PWO, Black LP (2000) Metamorphic zircon formation by solid state recrystallization of protolith igneous zircon. J Metamorph Geol 18:423–439

Kelly NM, Harley SL (2005) An integrated microtextural and chemical approach to zircon geochronology: refining the Archaean history of the Napier Complex, east Antarctica. Contrib Mineral Petrol 149: 57–84

Kretz R (1983) Symbols for rock-forming minerals. Am Mineral 68:277–279

Lavreau J, Poidevin JL, Ledent D, Liegeois JP, Weis D (1990) Contribution to the geochronology of the basement of Central African Republic. J Afr Earth Sci 11(1-2):69–82

Le Maître RW (1976) The chemical variability of some common rocks. J Petrol 17(4):589–637

Leeman WP, Budahan JP, Gerlach DC, Smith DR, Powell BN (1980) Origin of Hawaiian tholeiites: trace element contraints. Am J Sci 280(A):794–819

Mapoka H, Danguéné YPE, Nzenti JP, Biandja J, Kankeu B, Suh CE (2010) Major structural features and the tectonic evolution of the Bossangoa-Bossembele basement, Northwestern Central African Republic. Open Geol J 4:100–111

Miyashiro A (1974) Volcanic rock series in island arcs and active continental margins. Am J Sci 274:321–355

Ndema Mbongue JL, Ngnotue T, Ngo Nlend CD, Nzenti JP, Suh CE (2014) Origin and evolution of the formation of the Cameroon Nyong Series in the western border of the Congo craton. J Geosci Geomatics 2(2):62–75

Neves SP, Bruguier O, Vauchez A, Bosch D, Silva JMR, Mariano G (2006) Timing of crust formation, deposition of supracrustal sequences, and Transamazonian and Brasiliano metamorphism in the East Pernambuco belt (Borborema Province, NE Brazil): Implications for western Gondwana assembly. Precambrian Res 149:197–216

Nzenti JP (1998) L'Adamaoua panafricain (région de Banyo) : une zone clé pour un modèle de la chaîne panafricaine nord-équatoriale au Cameroun. Thèse Doctorat d'Etat, Université Cheikh Anta Diop -Université Nancy I, Sénégal-France

Nzenti JP, Barbey P, Macaudiere J, Soba D (1988) Origin and evolution of late Precambrian high - grade Yaoundé gneisses (Cameroon). Precambrian Res 38:91–109

Nzenti JP, Njiosseu TEL, Nzina NA (2007) The metamorphic evolution of the Paleoproterozoic high grade Banyo gneisses (Adamawa, Cameroon, Central Africa). J Cameroon Acad Sci 7:95–109

Osanai Y, Sajeev K, Owada M, Kehelpannala KVW, Prame WKB, Nakano N, Jayatileke S (2006) Metamorphic evolution of high-pressure and ultrahigh-temperature granulites from the Highland Complex, Sri Lanka. J Asian Earth Sci 28:20–37

Pearce JA, Cann JR (1973) Tectonic settings of basic volcanic rocks determined using trace element analyses. Earth Planet Sci Lett 19: 290–300

Pidgeon RT (1992) Recrystallisation of oscillatory zoned zircon: some geochronological and petrological implications. Contrib Mineral Petrol 110:463–472

Pin C, Poidevin JL (1987) U-Pb zircon evidence of Pan-African granulites facies metamorphism in Central African Republic. A new interpretation of the high-grade series of the northern border of the Congo Craton. Precambrian Res 36:302–312

Rolin P (1992) Présence d'un chevauchement ductile majeur d'âge panafricain dans la partie centrale de la République centrafricaine. Résultats préliminaires. C R Acad Sci Paris 315(2):467–470

Schaltegger U, Fanning CM, Günther D, Maurin JC, Schulmann K, Gebauer D (1999) Growth, annealing and recrystallization of zircon and preservation of monazite in high-grade metamorphism: conventional and in-situ U-Pb isotope, cathodoluminescence and microchemical evidence. Contrib Mineral Petrol 134:186–201

Shibata T, Thompson G, Frey FA (1979) Tholeiitic and alkali basalts from the middle Atlantic ridge at 43°N. Contrib Mineral Petrol 70: 127–142

Spear FS (1993) Metamorphic phase equilibria and pressure-temperature-time paths. Mineralogical Society of America, Monograph, pp 393–446

Spear FS, Cheney JT (1989) A petrogenetic grid for pelitic schists in the system SiO_2-Al_2O_3-FeO-MgO-K_2O-H_2O. Contrib Mineral Petrol 101:149–164

Spear FS, Kohn MJ, Cheney JT (1999) P-T paths from anatectic pelites. Contrib Mineral Petrol 134:17–32

Steiger RH, Jäger E (1977) Subcommision on geochronology: convention on the use of decay constants in geo-and cosmochronology. Earth Planet Sci Lett 36:369–362

Tanko Njiosseu TEL, Nzenti JP, Njanko T, Kapajika B, Nedelec A (2005) New U-Pb zircon ages from Tonga (Cameroon): coexisting Eburnean-Transamazonian (2.1 Ga) and Pan-African (0.6 Ga) imprints. C R Geosci 337(6):551–562

Taylor SR, McLennan SM (1981) The rare earth element evidence in Precambrian sedimentary rocks: implications for crustal evolution. In: Precambrian Plate Tectonics, Kröner edn. Elsevier, pp 527–548

Taylor SR, McLennan SM (1985) The continental crust: its composition and evolution. Blackwell, London 312 p

Thompson RN, Morrisson MA, Hendry GL, Parry SJ (1984) An assessment of the relative role of crust and mantle in magma genesis. An element approach. Philos Trans R Soc Lond A 310:549–590

Poidevin JL (1991) Les ceintures de roches vertes de la République Centrafricaine (Mboumou, Bandas, Boufoyo, Bogoin). Contribution à la connaissance du Précambrien du Nord du craton du Congo. Thèse de Doctorat d'Etat Université Clermont-Ferrand p. 440

Van de Camp PC, Leake BE, Senio A (1976) The petrography and geochemistry of some Californian arkoses with application to identifying of metasedimentary origin. J Geol 84:195–212

Van Schmus WR, Fetter AH, Brito Neves BB, Williams IS (1999) Ages of detrital zircon populations from Neoproterozoic supracrustal units in NE Brazil: implications for assembly of west Gondwanaland. Geol. Soc. Am. Abstr. Programs 31, 7, A-299, Denver, CO

Vavra G, Gebauer D, Schmid R, Compston W (1996) Multiple zircon growth and recrystallization during polyphase Late Carboniferous to Triassic metamorphism in granulites of the Ivrea Zone (Southern Alps): an ion microprobe (SHRIMP) study. Contrib Mineral Petrol 122:337–358

Vavra G, Schmid R, Gebauer D (1999) Internal morphology, habit and U-Th-Pb microanalysis of amphibolite-to-granulite facies zircons: geochronology of the Ivrea Zone (Southern Alps). Contrib Mineral Petrol 134:380–404

Vielzeuf D, Clemens JD (1992) The fluid-absent melting of phlogopite + quartz: experiments and models. Am Mineral 77:1206–1222

Williams IS, Claesson S (1987) Isotopic evidence for the Precambrian provenance and Caledonian metamorphism of high-grade paragneiss from the Seve Nappes, Scandinavian Caledonides. Contrib Mineral Petrol 97:205–217

Witt-Eickschen G, Seck HA, Mezger K, Eggins SM, Altheer R (2003) Lithospheric mantle evolution beneath the Eifel (Germany): constraints from Sr-Nd-Pb isotopes and trace element abundances in spinel peridotite and pyroxenites xenoliths. J Petrol 44:1077–1095